**Atmospheric
Chemistry
and Physics
Discussions**

Seasonal and spatial variability of surface ozone over China: contributions from background and domestic pollution

Y. Wang[1], Y. Zhang[1], J. Hao[1], and M. Luo[2]

[1]Department of Environmental Science and Engineering and State Key Joint Laboratory of Environment Simulation and Pollution, Tsinghua University, Beijing, China
[2]Jet Propulsion Laboratory, California Institute of Technology, Pasadena, California, USA

Correspondence to: Y. Wang (yxw@tsinghua.edu.cn)

ACPD

10, 27853–27891, 2010

Seasonal and spatial variability of surface ozone over China

Y. Wang et al.

Title Page

Abstract	Introduction
Conclusions	References
Tables	Figures

|◄ | ►|
◄ | ►

Back | Close

Full Screen / Esc

Printer-friendly Version

Interactive Discussion

Abstract

Both observations and a 3-D chemical transport model suggest that surface ozone over populated eastern China features a significant drop in mid-summer and that the peak month differs by latitude and region. Source-receptor analysis is used to quantify the contributions of background ozone and Chinese anthropogenic emissions on this variability. Annual mean background ozone over China shows a spatial gradient from 55 ppbv in the northwest to 20 ppbv in the southeast, corresponding with changes in topography and ozone lifetime. Anthropogenic background (annual mean of 12.6 ppbv) shows distinct troughs in the summer and peaks in the spring. On the monthly-mean basis, Chinese pollution ozone (CPO) has a peak of 20–25 ppbv in June north of the Yangtze River and in October south of it, which explains the peaks of surface ozone in these months. The mid-summer drop in ozone over eastern China is driven by the decrease of background ozone (-15 ppbv). Tagged simulations suggest that this decrease is driven by reduced transport from Europe and North America, whereas ozone from Southeast Asia and Pacific Ocean exhibits a maximum in the summer over eastern China. This contrast in seasonality provides clear evidence that the seasonal switch in monsoonal wind patterns plays a significant role in determining the seasonality of background ozone over China.

1 Introduction

Many nations set ambient air quality standards for surface ozone and regulate anthropogenic emissions of ozone precursors in order to protect public health and vegetation from the adverse effects of ozone pollution. Domestic pollution controls, however, will have little effect on the amount of ozone subsided or advected horizontally from outside the boundary layer. The background represents not only the natural concentrations of O_3 (the natural background produced from natural precursor sources or originated from the stratosphere) but also contributions from the long-range transport of O_3 produced

Full Screen / Esc

Printer-friendly Version

Interactive Discussion

from non-domestic anthropogenic emissions. Through global model simulations, background ozone over the US is estimated at 15–35 ppbv in the summer, including important contributions from anthropogenic pollutions of neighboring countries (Fiore et al., 2002; H. Wang et al., 2008).

The rising emissions from fossil fuel combustion in China are expected to increase surface concentrations of O_3 over the source region as well as the background of O_3 over other parts of the world. Despite the importance of changing anthropogenic emissions in China on the budget of tropospheric ozone over East Asia and globally, some fundamental understanding about ozone, such as its origin, spatial distribution, and seasonal variations, has yet to be studied through combined efforts of observation and modeling for China. Seasonal variations in surface ozone have been measured at a limited number of Chinese sites. Although these observations tend to suggest seasonal patterns different from site to site, they share one common feature that surface ozone over China does not have a distinct peak in mid-summer (July or August) in contrast to the pattern observed typically in the US. Surface ozone observed at a rural site (Miyun) near Beijing in July was found to have a good anti-correlation with cloud optical depths retrieved from MODIS (Y. Wang et al., 2008). Lin et al. (2009) conducted multi-scale model simulations of boundary layer ozone over East Asia and evaluated models' performance in response to the choice of chemical mechanism, dynamics and resolution. They found that simulation of summertime ozone over central east China is highly sensitive to the treatment of cloud cover and rainfall in the model. Although these studies demonstrated that summertime ozone over China is strongly influenced by the summer monsoonal circulation, the underlying mechanism has not been well quantified. A question of interest is the extent to which summer monsoon affects in situ production of ozone from regional sources as well as the transport of ozone from outside. A quantitative understanding of the relative contributions from the background and domestic anthropogenic sources on surface ozone over China will shed some light to this topic. It also has important implications for risk assessment and control strategies. After all, China is susceptible to anthropogenic emissions from other regions, in

particular Europe (Newell and Evans, 2000) and neighboring countries in Asia. Several studies have examined the contributions from European anthropogenic emissions to the background O_3 over Japan (Wild and Akimoto, 2001; Akimoto, 2003; Wild et al., 2004) and to the Asian outflow to the Pacific (Bey et al., 2001b; Liu et al., 2002), but little analysis has been conducted for their impacts on the background O_3 over China.

The present study uses a 3-D global model of tropospheric chemistry (GEOS-Chem) and its nested-grid version over East Asia to investigate some general features of the seasonal and spatial variations of surface O_3 over China and to identify contributions of various source types (natural and anthropogenic) and regions (domestic and foreign) to its spatial distribution and seasonality. We begin in Sect. 2 by describing the atmospheric chemistry transport model adopted in our study. We then examine in Sect. 3 the ability of the model to reproduce key features of ozone observed upwind, downwind, and within China. Source-receptor analysis is conducted in Sect. 4 to quantify the contributions from background and domestic anthropogenic emissions on the spatial and seasonal patterns of surface ozone over China. In Sect. 5, tagged tracer simulations are discussed to evaluate the contributions on surface ozone by source regions. The concluding remarks are given in Sect. 6.

2   Model description

The nested-grid GEOS-Chem model of tropospheric chemistry developed by Wang et al. (2004a) and Chen et al. (2009) is employed in the present study. The GEOS-Chem model is driven by meteorological data assimilated by the Goddard Earth Observing System (GEOS) at the NASA Global Modeling and Assimilation Office (GMAO). The present study uses GEOS-5 meteorology covering the period from December 2004 to present. The GEOS-Chem model includes a detailed tropospheric O_3-NO_x-hydrocarbon-aerosol simulation. The aerosol and oxidant chemistry are coupled through the formation of sulfate and nitrate, heterogeneous chemistry, and aerosol effects on photolysis rates (Bey et al., 2001a; Park et al., 2004). The structure of the

Seasonal and spatial variability of surface ozone over China

Y. Wang et al.

Full Screen / Esc

Printer-friendly Version

Interactive Discussion

nested-grid GEOS-Chem model involves a window with a uniform horizontal resolution of $0.5° \times 0.667°$ embedded in a low-resolution ($4° \times 5°$) global background. The nested-grid GEOS-Chem retains the generic high horizontal resolution of the GEOS-5 data over the nested regional domain. For the present study, the nested domain is set at 70° E–150° E and 11° S–55° N and includes all of China, its neighboring countries, and a significant portion of the northwestern Pacific. The high-resolution regional simulation is coupled dynamically to the low-resolution global model through lateral boundary conditions that are updated every three hours.

GEOS-Chem global runs uses national emission inventories for anthropogenic sources where available, and otherwise the base emission inventory of 1985 from the Global Emission Inventory Activity (GEIA) (Benkovitz et al., 1996) for NO_x, the non-methane hydrocarbon inventory from Piccot et al. (1992), and the CO emissions from Wang et al. (1998). Anthropogenic emissions of NO_x, CO, SO_2, and VOCs over East Asia were taken from the bottom-up inventory of Streets et al. (2003) for 2001 and Zhang et al. (2009) for 2006. Soil NO_x emissions are computed in GEOS-Chem using a modified version of the algorithm proposed by Yienger and Levy (1995). The exception is for east China, for which the model includes seasonally resolved soil NO_x emissions ($1.63\,Tg\,N\,yr^{-1}$) derived based on multi-year GOME satellite observations of tropospheric NO_2 columns up to 2000 (Wang et al., 2007a). Lightning emissions follow Price and Rind (1992), with the NO_x shape profile proposed by Pickering et al. (1998). The monthly flash rate is constrained by the monthly climatology for 1995–2005 based on the OTD/LIS measurements, while the flash rate and location within the month is allowed to vary with convection (Sauvage et al., 2007). Biomass burning emissions are taken from the GFED-2 inventory (van der Werf et al., 2006). Biogenic emissions of NMVOCs are adopted from the MEGAN inventory (Guenther et al., 2006).

3 Model evaluation

Application and evaluation of the GEOS-Chem model over and around China has been described by Wang et al. (2004a,b; 2007a,b) for CO and species of the reactive nitrogen family. In this work, we focus our evaluation on O_3 in order to diagnose the strengths and weakness in the model through comparisons with the following observations. The ability of the model to simulate seasonal variations in CO is presented as an additional evaluation of the model's transport. For model evaluation, we focus on the nested-grid model results for 2001 and 2006 when observations were available.

3.1 Surface O_3 and CO in East Siberia

Continuous measurements of O_3 and CO were made for three years (1997–1999) at Mondy (51°39′ N, 100°55′ E, 2006 m a.s.l.), a remote mountain site in East Siberia (Pochanart et al., 2003). Measurements at the Mondy site have been analyzed to define the inflow of trace gases to the East Asia Pacific rim region (Pochanart et al., 2003) and to quantify the trans-Eurasian international transport of air pollutants from Europe to East Asia (Wild et al., 2004). Figure 1 compares nested simulated and observed monthly-mean concentrations of O_3 (Fig. 1a) and CO (Fig. 1b) at the Mondy site. Monthly mean O_3 peaks in spring with a minimum in late summer early fall. Monthly mean CO has a maximum in spring and minimum in summer. Pochanart et al. (2003) attributed the spring maximum of CO at Mondy to the impact of forest fires in Siberia. The model successfully reproduces the mean mixing ratios of both species as well as their seasonal variations. There are minor negative biases (about −3 ppb) for O_3 except in winter. CO is well reproduced by the model for most months. Only notable discrepancies are a negative bias of 20 ppbv in December and positive bias of 20 ppbv in January. The discrepancy may be due partly to the fact that the model results (2001) are not sampled for the specific time when measurements were made (1997–1999). As the Mondy site is located close to the northwest boundary of the nested domain, the comparison leads confidence to the dynamic boundary conditions

provided from the global low-resolution simulation and verifies that the configuration of the nested-grid simulation adopted here is suitable for studying the intercontinental transport of pollutants from Europe to East Asia.

3.2 Seasonal variations of O_3 and CO at Chinese sites

Year-round measurements of O_3 and CO at only a few non-urban sites in China are available from literature. We selected three representative surface sites for model comparison: a remote coastal site (Hok Tsui) in Hong Kong (22°13′ N, 114°15′ E, 60 m a.s.l.) (Wang et al., 2009), a rural site (Lin An) in the Yangtze River Delta region (30°25′ N, 119°44′ E, 132 m a.s.l.) (Wang et al., 2001, 2002), and a rural site (Miyun) in the North China Plain (40°29′ N, 116°46.45′ E, 152 m a.s.l.) (Y. Wang et al., 2008, 2010b). The three sites, which are roughly 10° latitude apart and spread from south to north China, cover three fast-developing regions in China, namely the Pearl River Delta, Yangtze River Delta, and the Beijing-Tianjin-Tangshan city clusters. In addition, monthly-mean ozone observations at three mountain sites are also used: Mount Tai (36.25° N, 117.10° E, 1533 m a.s.l.), Mount Hua (34.49° N, 110.09° E, 2064 m a.s.l.) and Mount Huang (30.13° N, 118.15° E, 1836 m a.s.l.), all located in east China with continuous measurements of ozone from March 2004 to February 2005 (Li et al., 2007).

Seasonality of surface CO and O_3 at these sites is summarized in Fig. 2, with observations shown in upper panel and model results in lower panel. Monthly mean CO observed at the three surface sites (Fig. 2a) exhibits maxima in winter, resulting from increased lifetime of CO coupled with enhancement in regional emissions from residential heating. CO at Hok Tsui and Lin An has a minima in summer, while CO peaks in July at Miyun resulting from seasonal burning of crop residues after the harvest of winter wheat (Y. Wang et al., 2008, 2010b). Surface ozone exhibits distinctively different seasonality at the three surface sites (Fig. 2b). It peaks in autumn at Hok Tsui, in May at Lin An, and in June at Miyun. At the peak month, mean mixing ratio of O_3 increases from south to north, from 48 ppbv at Hok Tsui, to 58 ppbv at Lin An, and to 67 ppbv at Miyun. In contrast to the pattern observed typically in North America and

Europe (maxima in summer), a common feature of the three sites is the relatively low O_3 levels in middle summer months (July–August). The inflow of clean maritime air in the summer is one explanation for the mid-summer trough, as CO exhibits minima in the summer. Ozone observation at Mt. Tai and Mt. Hua (Fig. 2c) shows a peak in June and a low value in August, similar to surface ozone seasonality observed at Miyun as they are all located north of the Yangtze River. Ozone at Mt. Huang exists at peak values both in late spring and autumn, similar to that at the Lin An site.

The model successfully reproduces not only the general features in seasonality of both O_3 and CO at both surface and mountain sites, but also the gradients in both species between them (Fig. 2d–f). Annual mean levels of both CO and O_3 simulated by the model decrease from south to north, consistent with observations. The trough of both species in mid-summer months is well captured by the model. Major deficiencies in model CO simulations include underestimation of CO at all of the three sites except in the summer. This could be explained by the model's underestimate of CO emissions in these seasons. For ozone, the model overestimates the minima concentration levels in summer while it underestimates the duration of the summer trough. The discrepancy is probably due to the model's overestimate of ozone in marine boundary layers (Liu et al., 2006) and the model's inability to simulate cloud optical properties associated with the summer monsoon (Y. Wang et al., 2008). In addition, the fact that the model results (2006) were not sampled for the specific time when the measurements were made could explain part of the discrepancies between model results and observations.

3.3 Aircraft observations of O_3 in springtime outflow from China

The TRACE-P mission was conducted over the period of March–April 2001 with an objective to characterize the outflow of chemicals from Asia in the spring (Jacob et al., 2003). Two aircraft (DC-8 and P3-B) sampled a wide range of locations over the Western Pacific from bases in Hong Kong and Japan. Wang et al. (2004a,b) reported extensive comparisons of concentrations of CO and NO_y species obtained using the nested-grid model with results from the TRACE-P aircraft mission. The model was

shown to capture observed spatial variances of CO and NO_y, but to underestimate their concentrations for the boundary layer north 20° N due primarily to an underestimate of Chinese emissions of CO and NO_x.

Figure 3 compares the mean vertical profile of O_3 simulated using the nested-grid model with observations made in TRACE-P for a region north of 20° N and west of 150° E where the outflow from China was extensively sampled. The model results were based on simulations of 2001 meteorology and emissions (Streets et al., 2003). The observational results are indicated by red dots with red vertical lines denoting means and 1-σ standard deviations respectively. Model results (black lines) are presented in terms of means evaluated for specific flight times and locations. The model satisfactorily captures the observed vertical gradient and reproduces O_3 mixing ratios throughout the troposphere, with a minor negative bias (<3 ppb) below 1 km.

3.4 Seasonality of tropospheric O_3 retrieved by TES

As ground-level ozone is coupled with ozone's abundance in the troposphere, it is necessary to evaluate the model's performance in simulating the seasonality of tropospheric ozone column (TOC) over China. Satellite retrieval of TOC provides a valuable dataset for this purpose as few ozonesonde observations are available over China. Here we adopted TOC products retrieved from Tropospheric Emission Spectrometer (TES) aboard the NASA Aura satellite (Beer, 2006; Wang et al., 2010). TES standard products, global surveys, consists of 16 orbits of nadir vertical profiles every other day and provide 1–3 pieces of information for CO and ozone in the troposphere (Luo et al., 2007; Nassar et al., 2008). TES version 3 level-2 TOC derived from retrieved profiles during a period of three years (2006–2008) are used. As the present study focuses on regional and seasonal instead of episodic features of ozone over China, monthly mean TES TOC is averaged over two Chinese regions, east and west of China, defined as Chinese domains east and west of 110° E respectively.

Figure 4 compares the month to month variation of mean TOC over east (Fig. 4a) and west (Fig. 4b) China simulated by the model with that retrieved from TES. In the figure,

the monthly variability is calculated by subtracting annual mean TOC from monthly mean. TES retrievals suggest that TOC over both east and west China has a maximum in late spring/early summer and minimum in winter. This general seasonality in TOC is successfully reproduced by the model, but the model's maximum of TOC appears to occur 1–2 months earlier than TES. The seasonal amplitude in TOC is particularly consistent between the model and TES over east China. Over west China, however, the model underestimates the peak in the spring retrieved by TES. TES indicates a secondary peak of TOC in the fall over east China which is well captured by the model.

3.5 Summary of model evaluation

Several problems with the model were identified. First, the model has a minor low bias in simulating O_3 mixing ratio at the upwind site, Mondy, during maximal inflow seasons (winter and spring). This implies that our model analysis on the trans-Eurasian transport of O_3 may be a lower estimate. Second, the model may underestimate CO emissions and likely other ozone precursor emissions over China. Third, due to deficiencies in the emission data and the resolution of the model, it cannot reproduce the full extent of variability in ozone observations. The model tends to underestimate high ozone peaks and overestimate trough O_3 levels at a few sites.

However, we can see that the model captures the general seasonal pattern in O_3 and CO at the surface for locations upwind, downwind, and within China. The latitudinal gradient of both species inside China is well reproduced by the model. The evaluation against observations from the TRACE-P aircraft mission and TES satellite instruments lends confidence to the model's ability in simulating O_3 above the boundary layer.

4 Surface ozone by source category

With confidence established by the previous section to the model's ability in simulating key features of ozone observed over China, we apply model sensitivity analyses to

quantify the contributions from background and domestic anthropogenic emissions on the spatial and seasonal patterns of surface ozone over China.

4.1 Mean background

The simulation using emissions described in Sect. 2 is referred to as the standard simulation. Two sensitivity simulations were conducted in which we removed all anthropogenic emissions of NO_x, CO, and nonmethane hydrocarbons (1) within China, or (2) globally both in the nested-grid model and in the coarser-resolution global model which provides proper boundary conditions. Natural sources (NO_x from soil and lightning, biogenic VOCs, etc.) and biomass burning emissions remain unchanged. Sensitivity simulation 1 gives ozone levels that would exist in the absence of Chinese anthropogenic emissions, that is, total background O_3 (TBO) over China. Sensitivity simulation 2 gives the natural background of O_3 (NBO) over China, while the differences between sensitivity 1 and 2 represent pollution background O_3 (PBO) or the enhancement of O_3 resulting from anthropogenic emissions outside of China. The differences between the standard simulation and sensitivity simulation 1 are attributed to the ozone enhancement due to Chinese anthropogenic emissions, referred to as Chinese pollution enhancement (CPO) in this study. Table 1 summarizes different sets of simulations conducted in this study. The modeling approach follows Fiore et al. (2002) and is similar to the concept of source-receptor analysis which describes the sensitivity of surface ozone to a change in emissions from a source region or source category. Based on this modeling approach, the following relationships will hold for surface ozone of the standard simulation (referred hereafter as to total ozone or TO): TO = TBO + CPO, where TBO = NBO + PBO.

Table 2 summarizes mean and spatial variability of surface ozone averaged over China as a whole by season. Annual mean TBO over China is 44.1 ppbv, with maximum in spring (50.7 ppbv) and minimum in summer (40.9 ppbv), accounting for 93% and 81% of total surface ozone in these seasons respectively. Fiore et al. (2002) suggested that mean background ozone over the US is 20–45 ppb in the summer. In all seasons,

at least 70% of TBO is of natural origin. Mean NBO ranges from 29.0 ppbv in the fall to 35.9 ppbv in the spring, with an annual mean of 31.5 ppbv. The peak of NBO in the spring can be attributed to enhanced stratosphere-troposphere exchange (STE) activities in this season over Northern Hemisphere. Mean PBO ranges from 10.0 ppbv in the summer to 14.8 ppbv in the spring, with an annual mean of 12.6 ppbv. The spatial variability of background ozone is largest in the summer, as background ozone arising from biogenic emissions of NO_x and VOCs which peak in the summer is not necessarily collocated with stratospheric ozone or pollution background. Mean CPO ranges from 9.9 ppbv in the summer to only 1.4 ppbv in winter. For all of China, CPO contributes an average of about 20% of TO in the summer. However, the spatial variability in CPO reaches up to 100% compared with only 20% of variability in TO, suggesting CPO may account for much larger fractions over regions of large local emissions. The spatial variability in CPO exceeds 100% in the winter, as the model indicates negative CPO for northern regions in this season. With limited production of OH radicals in the winter at higher latitudes, enhancement in anthropogenic NO_x emissions will lead to ozone destruction through the so-called titration mechanism ($NO + O_3 \longrightarrow NO_2 + O_2$).

4.2 Spatial distributions

Spatial distributions of surface ozone and its different components for annual mean and summertime (JJA) conditions are presented in Figs. 5 and 6 respectively. Annual mean ozone concentrations (Fig. 5a) are relatively high (>50 ppb) over a zonal band extending from the elevated Tibetan Plateau in the west to central-east China (between 25° and 40° N). The high-O_3 band expands northward and westward in summer (Fig. 6a), with highest concentrations (>60 ppb) shifted to North China Plain where anthropogenic emissions are large. TBO is highest over western China (west of 100° E), accounting for about 90% of total surface ozone abundance both annually and in summer (Figs. 5b and 6b). TBO shows a distinct spatial gradient over China, decreasing from northwest to southeast. This gradient of TBO is largest in the summer (Fig. 6b), decreasing from 55 ppb over west China to less than 30 ppbv over southeast China.

The NBO (Figs. 5c and 6c) resembles the spatial distribution of TBO, as NBO is the dominant component of TBO. In contrast, the CPO is highest over eastern China where anthropogenic emissions are large (Figs. 5e and 6e).

The abundance of PBO at the surface (Figs. 5d and 6d) is much lower than NBO. The spatial distribution of PBO is different than TBO or NBO. It is relatively high over the coastal zones and southwest China because of the region's proximity to pollutions from neighboring countries/regions such as Japan, Korea, Southeast Asia and South Asia. PBO over China is on average 5 ppbv lower in the summer compared with annual mean, reflecting the influence of marine air inflow in summer. We will examine the factors resulting in the seasonal changes in the next Section.

Figure 7 presents the topography of China, illustrating the contrast in elevation between west and east China. Tibetan Plateau in the southwest has a mean elevation of over 3000 m, while Northwestern China (35–40° N, west of 110° E) has a mean elevation of about 2000 m. In contrast, the plain regions in central east and the hilly regions in southeast are of elevations lower than 500 m and 1000 m respectively. On one hand, the relatively high NBO and thus TBO over west China can be attributed to stratospheric influences because of the high altitude. On the other hand, it can be explained by spatial variability in ozone lifetime. The mean lifetime of ozone in the mixed layer against dry deposition and chemical losses over China in the summer is presented in Fig. 8. The chemical loss rates are calculated for the extended odd oxygen family ($O_x = O_3 + O + NO_2 + 2NO_3 + PANs + HNO_4 + HNO_3 + 3N_2O_5$) as in Fiore et al. (2002). O_x is hereafter referred to as O_3 since O_3 usually accounts for over 95% of O_x. The mean lifetime of O_3 in the mixed layer is greater than 5 days over the arid Loess Plateau in northwest China and over parts of the Tibetan Plateau. The lifetime in East China is typically less than 2 days, reflecting shallow mixing depth, faster deposition velocities, and more active chemical loss due to higher emissions of biogenic hydrocarbons and higher humidity. The strong northwest-to-southeast gradient in the lifetime of ozone is significant also in other seasons, resulting in the reduced concentrations of TBO and NBO over eastern China. The gradient in ozone lifetime coincides

with the spatial gradient in topography and other meteorological/geophysical parameters (such as precipitation, vegetation coverage, etc.). Our analysis is consistent with the study of Fiore et al. (2002) in which they found that the background of O_3 was generally higher in the western United States than in the eastern US. because of the higher lifetime of O_3 in the west with the arid climate.

4.3 Seasonality

Careful analyses of the results from the standard simulation suggest that it is not appropriate to generalize one seasonal pattern for surface ozone that can fit for situations across all parts of China. Therefore, we focus our analysis for four different regions in China: West China (WC; defined as 25–45° N, west of 110° E), Northeastern China (NEC; 42–50° N, 120–135° E), North China (NC; 34–42° N, 110–120° E), and South China (SC; region between 22–34° N, 110–120° E). The definition of these regions, illustrated in Fig. 5a, partly follows the conventional division of geographical regions in China and partly reflects the spatial distribution of different ozone components shown in Figs. 5–6. West China refers to the region west of 110° E with high elevation and arid climate. Natural ozone background is relatively high over WC. South China includes the subtropical middle and lower Yangtze Plains and southeast coastal mountains and hills, while North China covers temperate North China Plain. SC and NC are conventionally divided by the Yangtze River. Both SC and NC have larger population, higher gross domestic production, and consequently larger anthropogenic pollutant emissions than WC or NEC. As a result, the CPO is highest over NC and SC. Northeast China is at higher latitude with humid temperate climate. It is closet to European pollutions.

Figure 9a–d summarizes the month-to-month variations of mean surface ozone (red circles) averaged over the four Chinese regions. Over WC, TO peaks in spring and reaches a minimum in summer. Over NEC, it peaks in spring and has its minimum in winter. TO over NC reaches a maximum in June, only to decrease significantly in July. This is consistent with the seasonality of ozone observed at Miyun site (Wang et al., 2008, 2010b) and Mt. Tai (Li et al., 2007). TO over SC has a distinct double-hump

shape, with peaks in the fall and spring and minimum in summer, similar to observations at the Lin An and Hong Kong sites. Annual mean surface ozone is highest over NC, followed in order by WC, SC, and NEC. Mean springtime ozone is highest over WC, while in summertime it is highest over NC and lowest over SC.

Seasonality of individual ozone components displayed in Fig. 9 provides useful evidence for identifying important factors controlling the seasonal variability of surface ozone over different regions. NBO show distinct peaks in the spring over all four regions, reflecting the influence of STE on natural ozone background over the northern middle latitudes. NBO is highest over WC and lowest over SC. It is the largest component of TO over WC and NEC all year round. The seasonal amplitude of NBO is about 10 ppbv over the four regions. PBO shows distinct troughs in summer over all four regions. This can be explained in part by the decrease in the lifetime of ozone and its precursors in summer (thus unfavorable for long-range transport) and in part by summer monsoonal circulation which brings marine air masses with lower ozone to China. The transport issue will be investigated in Sect. 5 using the tagged ozone simulation. Monthly mean PBO ranges from 5 to 17 ppb depending on region and season. The lowest PBO is over SC in the summer. PBO peaks in spring over all regions due to longer O_3 lifetime (Wang et al., 1998) and larger influx of European pollution (Wild et al., 2004). As the combination of NBO and PBO, TBO has a maximum in spring and minimum in summer over all four regions. In WC, the seasonality of TO is determined by that of TBO. The spring peak of TO over NEC and SC is attributable also to TBO.

In contrast to the spring peak of hemispheric pollution background (PBO), ozone originated from Chinese pollutions (CPO) peaks in the summer and fall. This reflects stronger in situ production of ozone from local/regional precursor emissions under warmer temperature and stronger solar radiation prevailing in these seasons. CPO over WC is nearly zero in the winter and spring. It increases to a mean level of 5 ppbv from July to October, still lower than either natural background or anthropogenic background ozone in these months as local anthropogenic sources are minimal over WC. Over NEC, CPO has higher concentrations extending from spring to autumn. It ranges

Full Screen / Esc

Printer-friendly Version

Interactive Discussion

from −2 ppbv in December/January to 15 ppbv in June. The negative value indicates limited production of OH radicals in this region in the winter to oxidize anthropogenic NO_x emissions leading to net production of ozone. Instead, enhancement in anthropogenic NO_x emissions will lead to ozone destruction through the titration reaction. Because of CPO's contribution, ozone minimum over NEC occurs in the winter instead of summer. The contribution of CPO to total ozone is much larger over NC and SC where anthropogenic emissions are large. Annual mean CPO over NC and SC is 8 and 11 ppbv respectively. Monthly mean CPO reaches up to 30 ppbv over NC in August and 25 ppbv over SC in September. Nevertheless, TBO still contributes for more than 50% of total surface ozone over NC and SC in all seasons. The relative importance between CPO and TBO on surface ozone is more complicated over NC and SC. As the two regions have dense population and higher level of economic development, we will discuss these two regions in more detail.

Over NC (Fig. 9c), monthly mean CPO exceeds 20 ppbv from June to September, with a maximum of 30 ppbv in August. Although TBO decreases by 5 ppbv from May to June, CPO increases by about 10 ppbv during the same period, leading to a maximum of TO (the sum of TBO and CPO) in June. TBO further decreases by 10 ppbv from June to July, while CPO increases by only 3 ppbv suggesting slower net in situ production of ozone in July compared with June. As a result, TO shows a decrease from June to July. From July to August, CPO increases by another 10 ppbv offsetting the 5 ppbv decrease in TBO, leading to a secondary peak of TO in August. Wang et al. (2008) attributed the decrease in surface O_3 from June to July at the Miyun site to increases in monsoonal rainfall and cloudiness in July as optically-thick clouds suppress photochemical production of O_3. The June-July-August variation in CPO identified here for NC as a whole may be explained by the same mechanism since July is the month when monsoonal rainfall reaches North China region.

Over SC (Fig. 9d), CPO peaks in the fall instead of summer, leading to the maximum of TO in the fall. Summer monsoon season has a longer duration over SC with heavy rainfall and extensive clouds. Although ozone production can be significant in days

when it is clear, the overall meteorology in summer is less favorable for in situ production and accumulation of ozone than in the fall when it is generally warm and sunny with little precipitation. The increase in CPO from spring to summer is only 5 ppbv, far from offsetting a large decrease of 20 ppbv in TBO during the same period. Therefore, total surface ozone still exhibits a summer minimal over SC, similar to TBO. Mean CPO is positive over SC in the winter, suggesting enough production of OH radical to oxidize anthropogenic NO_x emissions leading to net production of ozone. This is because at lower latitude, SC has mean temperature above freezing point and plenty of solar radiation even in winter.

5 Surface ozone by source region

The sensitivity simulation discussed in the previous section is an effective method to relate quantitatively surface ozone components to different source types of precursor emissions: natural versus anthropogenic, domestic pollution versus outside China. Due to computational constraints, however, the number of sensitivity simulations that can be conducted effectively is limited. In this section, we apply the tagging method to evaluate contributions on surface ozone by source region, as done by Fiore et al. (2002). 3-D fields of daily mean production and loss frequencies of the odd oxygen family (O_x; cf. Sect. 4.2) archived from our standard simulation are used to drive an off-line ozone simulation, in which ozone in the model is tagged by region of production. Total ozone is the sum of individual tagged tracers produced in different regions. Each tracer is subjected to the same chemical loss and dry deposition frequencies as the total O_3, but is produced only within its specific source region. This approach allows surface ozone over China to be decomposed into components produced from different source regions. We defined the following 11 source regions: four Chinese regions as described in Sect. 4.3, Europe (EU; defined as north of 38° N, 15° W–55° E), North America (NA; 20° N–75° N, 127° W–65° W), Southeast Asia (SEA; 10° S–22° N, 90° E–110° E, and 10° S–18° N, 110–130° E), India (IND; 6° N–38° N, 60° E–90° E), Japan and

Korea (JaKr; 30° N–54° N, 125° E–150° E), west of the Pacific Ocean (PA; 5° N–30° N, 130° E–160° E), and the rest of world (ROW). Except for ROW, each source region extends from the surface up to 2.5 km altitude or about 750 hPa, representing only the PBL. Ozone produced above 2.5 km is counted into ROW. Stratospheric injection is treated as a separate tracer. In what follows, a tagged region is referred to as the source region of its own tagged tracer, while the four Chinese regions are the receptor regions of interest in this paper. The sum of O_3 from all source regions is within a few percent of the total O_3 in the standard full chemistry simulation.

Figure 10 presents monthly mean concentrations of tagged O_3 tracers averaged over the four Chinese regions. We first discuss the Chinese tracers displayed on the left panels. The sum of tagged Chinese tracers (total CH O_3 for short), representing total ozone produced within the Chinese PBL, is shown as a filled black square. We should note here that total CH O_3 is larger than CPO derived from the sensitivity simulation (cf. Fig. 9) although they have very similar month-to-month variability. This is because the former accounts for ozone produced in PBL above China from all sources of precursors, either natural or anthropogenic or those originated from outside China, as long as they result in ozone production within the receptor region. From Fig. 10, one can see that ozone produced within the source region makes the biggest contribution to total surface ozone for the same region. For example, tagged NC O_3 (i.e., ozone produced over North China PBL) ranges from 7 ppbv in the winter to 38 ppbv in the summer over NC (Fig. 10a), compared with only 6 ppbv in the fall over the receptor region of SC (Fig. 10c). Chinese O_3 all peak in the summer over their source regions, with the only exception of SC O_3 which peaks in the fall over SC for reasons discussed before. The seasonality of Chinese O_3 over the receptor regions indicates transport pathways of ozone within China. NC O_3 reaches a peak level of 6 ppbv over SC in the fall, while a similar maximum level of SC O_3 is found over NC in late spring and early summer (May–June). This suggests that the fall season is the period of maximum export of ozone from NC to SC, while May to June is the period of largest export of ozone from SC to NC. These transport routes can be explained by the

prevailing southwesterly in the summer and northwesterly in the fall associated with the monsoonal circulation. This cross-regional transport of ozone between NC and SC provides an additional mechanism to explain why surface ozone peaks in June and in the fall, respectively, over NC and SC. Compared with NC or SC O_3, WC and NEC O_3 make significant contributions only at their source regions (Fig. 10e and g). In the summer when the prevailing wind is southwesterly, NC O_3 has its maximum influence over NEC, while SC O_3 reaches its peak over WC. Peak level of NC and SC O_3 is about 5.8 ppbv and 2.4 ppbv over NEC and WC respectively.

Monthly mean mixing ratios of selective non-Chinese tracers are shown on the right panels of Fig. 10. As these tracers represent the contribution of ozone produced outside Chinese PBL, their month-to-month variations shed some light on the impact of different source regions on the seasonality of background ozone discussed in Sect. 4.3. The abundance of EU O_3 decreases from north to south over China, with largest annual mean influence of 3.6 ppbv over NEC and lowest of 1.2 ppbv over SC. NA O_3 exhibits a similar pattern as EU O_3 but of lower mixing ratio, decreasing from an annual mean level of 2.6 ppbv over NEC to that of 1.2 ppbv over SC. EU O_3 tends to peak in the spring while NA O_3 often peaks in the winter. Compared with NA and EU, SEA O_3 has a smaller contribution of less than 1 ppbv all year round over NEC, NC, and WC. The exception is that SEA O_3 reaches 1.4–2.1 ppbv from April to July over SC, larger than NA or EU O_3. This is due to the shorter transport route from SEA to SC during this period under the prevailing southwesterly winds. The springtime enhancement of SEA O_3 is resulted from biomass burning that peaks in this season over Southeast Asia (Duncan et al., 2003).

The biggest influence of JaKr O_3 is over NEC, reaching 2–4.5 ppbv from April to August with an annual mean of 2 ppbv and a peak in June. It also has a significant contribution over NC and SC in the fall reaching up to 2 ppbv over both regions. Reflecting the prevailing wind directions, the receptor region of JaKr O_3 switches from NEC in the summer to NC/SC in the fall. Indian O_3 makes large contributions over WC all year round, with an annual mean of 4.5 ppbv exceeding those from EU or NA. It

peaks in the spring, again consistent with prevailing wind directions. Liu et al. (2009) defined region of primary influence (RPI) as the largest foreign source region to influence a receptor. From Fig. 10, we can see that on annual basis, RPI of ozone over NC, SC, NEC, and WC is EU, NA, EU, and IND respectively.

5   A common feature for all four Chinese receptor regions is that ozone exported from North American and Europe reaches a minimum in the summer. In contrast, ozone exported from SEA and PA exhibits a maximum in the summer over NC and SC, with negligible influence over the inland regions (i.e., WC and NEC). NA and EU O_3 in combination result in a decrease of 4–8 ppbv from spring to summer over different regions

10 in China, more than offsetting an increase of less than 2 ppb resulting from SEA and PA O_3 during the same period. O_3 from ROW contributes to a further decrease of about 8 ppbv from spring to winter. The contrast in seasonality between the tagged tracers provides clear evidence that it is the seasonal switch in monsoonal wind patterns that plays a significant role in determining the seasonality of background ozone over China.

15 The northwesterly monsoon brings polluted continental air masses with higher ozone levels in the spring and fall as represented by NA and EU O_3. It switches to southwesterly in the summer bringing in relatively clean marine air masses from the south. As a result, anthropogenic background ozone shows a distinct summer minimum over all regions of China. It also provides a second mechanism to explain the decrease in

20 natural background from spring to summer besides the role of stratospheric influence discussed above, as tagged ozone accounts for contributions from natural precursor emissions over source regions.

6 Concluding remarks

In this study, we use a nested-grid chemical transport model with a horizontal resolution

25 of 0.5° × 0.667° to quantify contributions of various source types (natural and anthropogenic) and regions (domestic and foreign) to the spatial distribution and seasonality of surface ozone over China. Surface observation, satellite-derived tropospheric ozone

Seasonal and spatial variability of surface ozone over China

Y. Wang et al.

column, and nested-grid model all suggests that surface ozone over populated eastern China features a significant drop in mid-summer. The peak month of surface ozone differs by latitude and region, changing from October in PRD to May in YRD and to June in NCP. With confidence in the model's ability in simulating key features of ozone observed upwind, downwind and over China, we apply model sensitivity analyses to decompose total surface ozone (TO) into contributions from total background ozone (TBO), natural background (NBO), pollution background (PBO), and the enhancement from Chinese anthropogenic pollutants (CPO). We found that TBO over China in all seasons has a large spatial gradient, annual mean TBO decreasing from 52 ppbv in the northwest to 33 ppbv in the southeast. This gradient is associated with changes in topography and ozone lifetime. NBO resembles the spatial distribution of TBO, as NBO is the dominant component of TBO. PBO is relatively high over the coastal zones and southwest China because of the proximity to pollutions from neighboring countries/regions. In contrast to background ozone, the CPO is highest over eastern China where anthropogenic emissions are large. When averaged over whole China, CPO contributes about 20% of TO in summer. However, the spatial variability in CPO reaches up to 100%, suggesting CPO may account for much larger fractions over regions with large emissions.

As it is not appropriate to generalize one seasonal pattern for surface ozone that can fit for all parts of China, we focus our analysis of seasonality over four different regions in China: West China (WC), Northeastern China (NEC), North China (NC), and South China (SC). NBO show distinct peaks in the spring over all four regions, reflecting the influence of STE on natural ozone background over the northern middle latitudes. In spring, NBO ranges from 45 ppbv averaged over WC to 30 ppbv over SC. The spring peak of surface ozone over WC and NEC is attributed to that of NBO. PBO shows distinct troughs in summer over all four regions. This can be explained in part by the decrease in the lifetime of ozone and its precursors in the summer and in part by summer monsoonal circulation which brings marine air masses with lower ozone to China. Monthly mean PBO ranges from 5 to 17 ppb depending on region and season. PBO peaks in the spring over all regions due to longer O_3 lifetime and larger influx

of European pollution. As the combination of NBO and PBO, TBO has a maximum in spring and minimum in summer over all four regions. On the monthly-mean basis, CPO exceeds anthropogenic background only in the summer and fall over NC and SC where domestic emissions are large. CPO peaks in June over NC (north of the Yangtz River) and in October over SC, resulting in corresponding peaks of surface ozone in these months over the two regions. The mid-summer drop in ozone over SC and NC is driven by the decrease of background ozone, although CPO shows an increase in the summer but of much less magnitude.

Tagged simulations suggest that the summertime decrease in background ozone is a result of reduced transport from Europe and North America, whereas ozone from Southeast Asia and Pacific Ocean exhibits a maximum in the summer. This contrast in seasonality provides clear evidence that it is the seasonal switch in monsoonal wind patterns that plays a significant role in determining the seasonality of background ozone over China. The northwesterly monsoon brings polluted continental air masses with higher ozone levels in the spring and fall. It switches to southwesterly in the summer bringing in relatively clean marine air masses from the south. As a result, anthropogenic background ozone shows a distinct summer minimum over all regions of China. The tagged ozone simulation indicates that the influence from foreign source regions differ in different receptor regions. On the annual basis, foreign region of primary influence on ozone over NC, SC, NEC, and WC is EU, NA, EU, and IND respectively. Ozone produced from the European boundary layer has the largest influence averaged over the entire China. Its maximum monthly-mean influence ranges from 2 ppb in SC to 6 ppb in NEC.

The focus of our analysis is on the influence of different source regions and source types on monthly-mean and regional-averaged abundance of surface ozone over China. Another aspect is on these source regions/types on the day-to-day variability of surface ozone and the implications on air quality management. Although it is not in the scope of our study, this topic is of great importance and will be studied in our subsequent research.

References

Akimoto, H.: Global air quality and pollution, Science, 302(5651), 1716–1719, 2003.

5 Beer, R.: TES on the Aura Mission: Scientific Objectives, Measurements, and Analysis Overview, IEEE T. Geosci. Remote, 44, 1102–1105, 2006.

Benkovitz, C. M., Scholtz, M. T., Pacyna, J., Tarrason, L., Dignon, J., Voldner, E. C., Spiro, P. A., Logan, J. A., and Graedel, T. E.: Global gridded inventories of anthropogenic emissions of sulfur and nitrogen, J. Geophys. Res., 101(D22), 29239–29253, 1996.

10 Bey, I., Jacob, D. J., Yantosca, R. M., Logan, J. A., Field, B. D., Fiore, A. M., Li, Q. B., Liu, H. Y., Mickley, L. J., and Schultz, M. G.: Global modeling of tropospheric chemistry with assimilated meteorology: Model description and evaluation, J. Geophys., Res., 106(D19), 23073–23095, 2001a.

Bey, I., Jacob, D. J., Logan, J. A., and Yantosca, R. M.: Asian chemical outflow to the Pacific

15 origins, pathways and budgets, J. Geophys. Res., 106(D19), 23097–23113, 2001b.

Chen, D., Wang, Y., McElroy, M. B., He, K., Yantosca, R. M., and Le Sager, P.: Regional CO pollution and export in China simulated by the high-resolution nested-grid GEOS-Chem model, Atmos. Chem. Phys., 9, 3825–3839, doi:10.5194/acp-9-3825-2009, 2009.

Ding, A. J., Wang, T., Thouret, V., Cammas, J.-P., and Nédélec, P.: Tropospheric ozone cli-

20 matology over Beijing: analysis of aircraft data from the MOZAIC program, Atmos. Chem. Phys., 8, 1–13, doi:10.5194/acp-8-1-2008, 2008.

Duncan, B. N., Martin, R. V., Staudt, A. C., Yevich, R., and Logan, J. A.: Interannual and seasonal variability of biomass burning emissions constrained by satellite observations, J. Geophys. Res., 108(D2), 4100, doi:10.1029/2002JD002378, 2003.

25 Fiore, A., Jacob, D. J., Bey, I., Yantosca, R. M., Field, B. D., Fusco, A. C., and Wilkinson, J. G.: Background ozone over the United States in summer: Origin, trend, and contribution to pollution episodes, J. Geophys. Res., 107, D154275, doi:10.1029/2001JD000982, 2002.

Fiore, A., Jacob, D. J., Liu, H., Yantosca, R. M., Fairlie, T. D., and Li, Q.: Variability in surface ozone background over the United States: Implications for air quality policy, J. Geophys.

30 Res., 108(D2), D244787, doi:10.1029/2003JD003855, 2003.

Seasonal and spatial variability of surface ozone over China

Y. Wang et al.

Title Page

Abstract	Introduction
Conclusions	References
Tables	Figures

|◄ | ►|

◄ | ►

Back | Close

Full Screen / Esc

Printer-friendly Version

Interactive Discussion

Guenther, A., Karl, T., Harley, P., Wiedinmyer, C., Palmer, P. I., and Geron, C.: Estimates of global terrestrial isoprene emissions using MEGAN (Model of Emissions of Gases and Aerosols from Nature), Atmos. Chem. Phys., 6, 3181–3210, doi:10.5194/acp-6-3181-2006, 2006.

Jacob, D. J., Crawford, J. H., Kleb, M. M., Connors, V. S., Bendura, R. J., Raper, J. L., Sachse, G. W., Gille, J. C., Emmons, L., and Heald, C. L.: Transport and Chemical Evolution over the Pacific (TRACE-P) aircraft mission: Design, execution, and first results, J. Geophys. Res., 108, D209000, doi:10.1029/2002JD003276, 2003.

Li, J., Wang, Z. F., Akimoto, H., Chao, G., Pochanart, P., and Wang, X.: Modeling study of ozone seasonal cycle in lower troposphere over east Asia, J. Geophys. Res., 112, D22S25, doi:10.1029/2006JD008209, 2007.

Lin, M., Holloway, T., Oki, T., Streets, D. G., and Richter, A.: Multi-scale model analysis of boundary layer ozone over East Asia, Atmos. Chem. Phys., 9, 3277–3301, doi:10.5194/acp-9-3277-2009, 2009.

Liu, H. Y., Jacob, D. J., Chan, L. Y., Oltmans, S. J., Bey, I., Yantosca, R. M., Harris, J. M., Duncan, B. N., and Martin, R. V.: Sources of tropospheric ozone along the Asian Pacific Rim: An analysis of ozonesonde observations, J. Geophys. Res., 107, D214573, doi:10.1029/2001JD002005, 2002.

Liu, J. F., Mauzerall, D. L., Horowitz, L. W., Ginoux, P., and Fiore, A. M.: Evaluating intercontinental transport of fine aerosols: (1) Methodology, global aerosol distribution and optical depth, Atmos. Environ., 43, 4327–4338, 2009.

Liu, X., Chance, K., Sioris, C. E., Kurosu, T. P., Spurr, R. J. D., et al.: First directly retrieved global distribution of tropospheric column ozone from GOME: Comparison with the GEOS-CHEM model, J. Geophys. Res., 111, D02308, doi:10.1029/2005JD006564, 2006.

Luo, M., Rinsland, C., Fisher, B., Sachse, G., et al.: TES carbon monoxide validation with DACOM aircraft measurements during INTEX-B 2006, J. Geophys. Res., 112, D24S48, doi:10.1029/2007JD008803, 2007.

Nassar, R., Logan, J. A., Worden, H. M., Megretskaia, I. A., Bowman, K. W., et al.: Validation of Tropospheric Emission Spectrometer (TES) nadir ozone profiles using ozonesonde measurements, J. Geophys. Res., 113, D15S17, doi:10.1029/2007JD008819, 2008.

Newell, R. E. and Evans, M. J.: Seasonal changes in pollutant transport to the North Pacific: the relative importance of Asian and European sources, Geophys. Res. Lett., 27(16), 2509–2512, 2000.

Seasonal and spatial variability of surface ozone over China

Y. Wang et al.

Title Page

Abstract	Introduction
Conclusions	References
Tables	Figures

| ◄◄ | ►► |
| ◄ | ► |

| Back | Close |

Full Screen / Esc

Printer-friendly Version

Interactive Discussion

Park, R. J., Jacob, D. J., Field, B. D., Yantosca, R. M., and Chin, M.: Natural and transboundary pollution influences on sulfate-nitrate-ammonium aerosols in the United States: Implications for policy, J. Geophys. Res., 109, D15204, doi:10.1029/2003JD004473, 2004.

Piccot, S. D., Watson, J. J., and Jones, J. W.: A Global inventory of volatile organic-compound emissions from anthropogenic sources, J. Geophys. Res., 97(D9), 9897–9912, 1992.

Pickering, K. E., Wang, Y., Tao, W. K., Price, C., and Müler, J. F.: Vertical distributions of lightning NO_x for use in regional and global chemical transport models, J. Geophys. Res., 103(D23), 31203–31216, 1998.

Pochanart, P., Akimoto, H., and Kajii, Y.: Regional background ozone and carbon monoxide variations in remote Siberia/East Asia, J. Geophys. Res., 108, D14028, doi:10.1029/2001JD001412, 2003.

Price, C. and Rind, D.: A Simple Lightning Parameterization for Calculating Global Lightning Distributions, J. Geophys. Res., 97(D9), 9919–9933, 1992.

Sauvage, B., Martin, R. V., van Donkelaar, A., Liu, X., Chance, K., Jaeglé, L., Palmer, P. I., Wu, S., and Fu, T.-M.: Remote sensed and in situ constraints on processes affecting tropical tropospheric ozone, Atmos. Chem. Phys., 7, 815–838, doi:10.5194/acp-7-815-2007, 2007.

Streets, D., Bond, T., Carmichael, G., et al.: An inventory of gaseous and primary aerosol emissions in Asia in the year 2000, J. Geophys. Res., 108(D21), 8809, doi:10.1029/2002JD003093, 2003.

van der Werf, G. R., Randerson, J. T., Giglio, L., Collatz, G. J., Kasibhatla, P. S., and Arellano Jr., A. F.: Interannual variability in global biomass burning emissions from 1997 to 2004, Atmos. Chem. Phys., 6, 3423–3441, doi:10.5194/acp-6-3423-2006, 2006.

Wang, H. Q., Jacob, D. J., Le, S. P., Streets, D. G., Park, R. J., Gilliland, A. B., and van Donkelaar, A.: Surface ozone background in the United States: Canadian and Mexican pollution influences, Atmos. Environ., 43(6), 1310–1319, 2008.

Wang, T., Cheung, V., Anson, C. M., and Li, Y. S.: Ozone and related gaseous pollutants in the boundary layer of eastern China: Overview of the recent measurements at a rural site, Geophys. Res. Lett., 28(12), 2373–2376, 2001.

Wang, T., Cheung, T. F., Li, Y. S., Xu, X. M., and Blake, D. R.: Emission characteristics of CO, NO_x, SO_2 and indications of biomass burning observed at a rural site in eastern China, J. Geophys. Res., 107(D12), 4157, doi:10.1029/2001JD000724, 2002.

Seasonal and spatial variability of surface ozone over China

Y. Wang et al.

Title Page

Abstract	Introduction
Conclusions	References
Tables	Figures

◀◀   ▶▶

◀   ▶

Back   Close

Full Screen / Esc

Printer-friendly Version

Interactive Discussion

Wang, T., Wei, X. L., Ding, A. J., Poon, C. N., Lam, K. S., Li, Y. S., Chan, L. Y., and Anson, M.: Increasing surface ozone concentrations in the background atmosphere of Southern China, 1994-2007, Atmos. Chem. Phys., 9, 6217–6227, doi:10.5194/acp-9-6217-2009, 2009.

Wang, Y. H., Jacob, D. J., and Logan, J. A.: Global simulation of tropospheric O_3-NO_x hydrocarbon chemistry, 1. Model formulation, J. Geophys, Res., 103(D9), 10713-10716, 1998.

Wang, Y. X., McElroy, M. B., Jacob, D. J., and Yantosca, R. M.: A nested grid formulation for chemical transport over Asia: Applications to CO, J. Geophys. Res., 109, D22307, doi:10.1029/2004JD005237, 2004a.

Wang, Y. X., McElroy, M. B., Wang, T., and Palmer, P. I.: Asian emissions of CO and NO_x: Constraints from aircraft and Chinese station data, J. Geophys. Res., 109, D24304, doi:10.1029/2004JD005250, 2004b.

Wang, Y. X., McElroy, M. B., Martin, R. V., Streets, D. G., Zhang, Q., and Fu, T. M.: Seasonal variability of NO_x emissions over east China constrained by satellite observations: Implications for combustion and microbial sources, J. Geophys. Res., 112, D06301, doi:10.1029/2006JD007538, 2007a.

Wang, Y. X., McElroy, M. B., Boersma, K. F., Eskes, H. J., and Veefkind, J. P.: Traffic restrictions associated with the Sino-African summit: Reductions of NO_x detected from space, Geophys. Res. Lett., 34, L08814, doi:10.1029/2007GL029326, 2007b.

Wang, Y., McElroy, M. B., Munger, J. W., Hao, J., Ma, H., Nielsen, C. P., and Chen, Y.: Variations of O_3 and CO in summertime at a rural site near Beijing, Atmos. Chem. Phys., 8, 6355–6363, doi:10.5194/acp-8-6355-2008, 2008.

Wang, Y. X., Zhang, Y., and Hao, J.: Review on the applications of Tropospheric Emissions Spectrometer to air-quality research: Perspectives for China, Frontiers of Environmental Science and Engineering in China, 4(1), 12–19, doi:10.1007/s11783-010-0012-9, 2010a.

Wang, Y., Munger, J. W., Xu, S., McElroy, M. B., Hao, J., Nielsen, C. P., and Ma, H.: CO_2 and its correlation with CO at a rural site near Beijing: implications for combustion efficiency in China, Atmos. Chem. Phys., 10, 8881–8897, doi:10.5194/acp-10-8881-2010, 2010b.

Wild, O. and Akimoto, H.: Intercontinental transport of ozone and its precursors in a three-dimensional global CTM, J. Geophys. Res., 106(D21), 27729–27744, 2001.

Wild, O., Pochanart, P., and Akimoto, H.: Trans-Eurasian transport of ozone and its precursors, J. Geophys. Res., 109, D11302, doi:10.1029/2003JD004501, 2004.

Seasonal and spatial variability of surface ozone over China

Y. Wang et al.

Title Page

Abstract	Introduction
Conclusions	References
Tables	Figures

|◀| |▶|

|◀| |▶|

Back | Close

Full Screen / Esc

Printer-friendly Version

Interactive Discussion

Xu, X., Lin, W., Wang, T., Yan, P., Tang, J., Meng, Z., and Wang, Y.: Long-term trend of surface ozone at a regional background station in eastern China 1991-2006: enhanced variability, Atmos. Chem. Phys., 8, 2595–2607, doi:10.5194/acp-8-2595-2008, 2008.

Yienger, J. J. and Levy, H.: Empirical model of global soil-biogenic NO_x emissions, J. Geophys. Res., 100(D6), 11447–11464, 1995.

Zhang, Q., Streets, D. G., Carmichael, G. R., He, K. B., Huo, H., Kannari, A., Klimont, Z., Park, I. S., Reddy, S., Fu, J. S., Chen, D., Duan, L., Lei, Y., Wang, L. T., and Yao, Z. L.: Asian emissions in 2006 for the NASA INTEX-B mission, Atmos. Chem. Phys., 9, 5131–5153, doi:10.5194/acp-9-5131-2009, 2009.

Seasonal and spatial variability of surface ozone over China

Y. Wang et al.

Title Page

Abstract	Introduction
Conclusions	References
Tables	Figures

◄ ►

◄ ►

| Back | Close |

Full Screen / Esc

Printer-friendly Version

Interactive Discussion

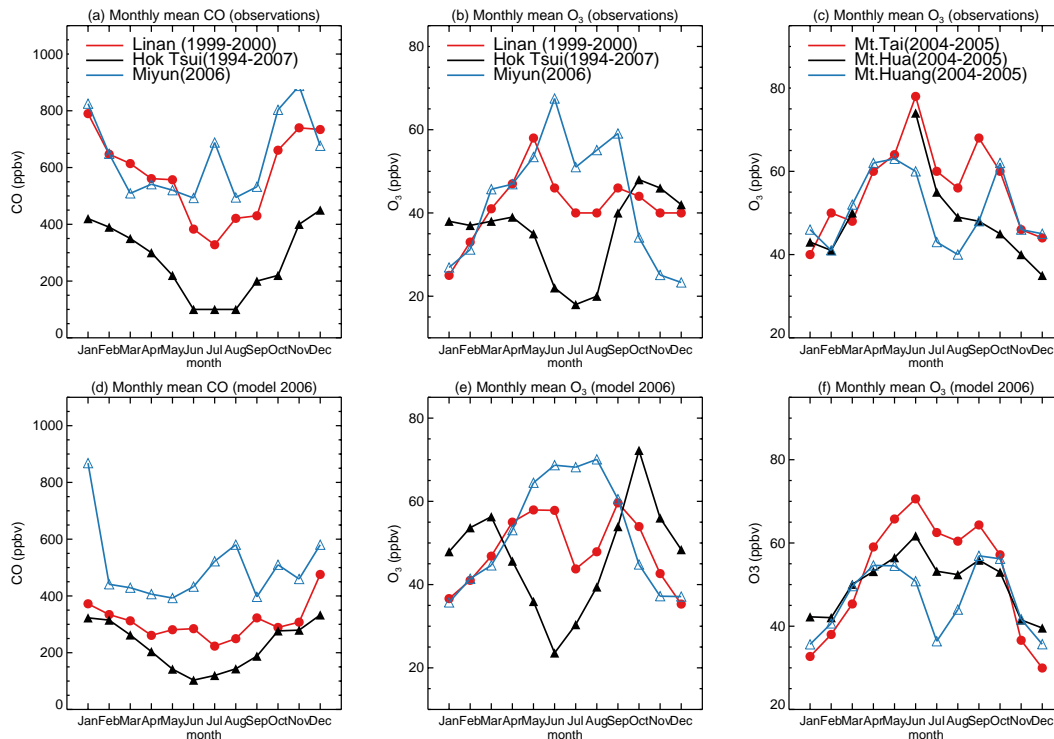**Seasonal and spatial variability of surface ozone over China**
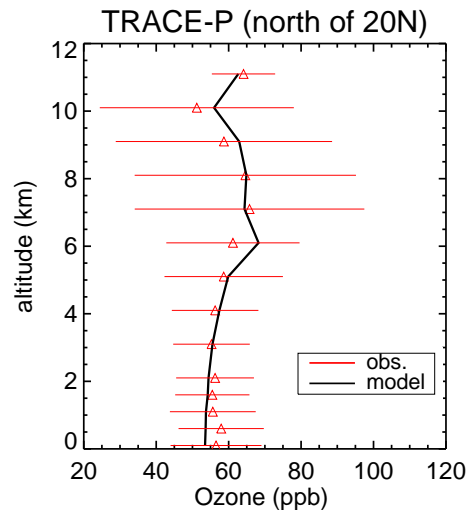
Y. Wang et al.

Table 1. Simulation used in the study.

Name	Description
1. Standard simulation	Anthropogenic and natural emissions as described in the text (Sect. 2).
2. China total background ozone	Same as 1 but without the Chinese anthropogenic emissions.
3. Natural background	Same as 1 but without the global anthropogenic simulation.
4. Tagged ozone simulation	Driven by daily production and loss frequency of ozone files archived from Simulation 1.

Table 2. Surface ozone and its decomposition averaged over China by season. Results are presented as mean ± spatial deviation (unit: ppbv).

Season	total ozone (TO)	Total background (TBO)	Natural background (NBO)	Pollution background (PBO)	China Pollution (CPO)
Winter (DJF)	44.4 ± 5.7	43 ± 5.9	30.2 ± 4.7	12.8 ± 1.5	1.4 ± 3.5
Spring (MAM)	54.7 ± 5.3	50.7 ± 8.6	35.9 ± 7.4	14.8 ± 2.2	4 ± 5.4
Summer (JJA)	50.8 ± 10.2	40.9 ± 12.9	30.9 ± 10.4	10 ± 4	9.9 ± 9.2
Fall (SON)	48.3 ± 6.2	41.7 ± 9	29 ± 6.8	12.7 ± 2.6	6.6 ± 7.5
Annual mean	49.5 ± 5.2	44.1 ± 8.5	31.5 ± 6.7	12.6 ± 2.3	5.4 ± 5

Fig. 1. Monthly mean O_3 **(a)** and CO **(b)** mixing ratios (ppbv) of observation (red circles) and model (black triangels) at the Mondy site.

Fig. 2. Monthly mean O_3 and CO at surface and mountain sites in China. The upper panels are the observation data, and the lower panels are the model results. The left panels (**a** and **d**) are CO data at Linan (red circles), Hok Tsui (black triangles) and Miyun (blue triangles); the middle two panels (**b** and **e**) are O_3 data at the same sites with the left panel; the right two panels (**c** and **f**) are O_3 data at Mt. Tai (red circles), Mt. Hua (black triangles), and Mt. Huang (blue triangles).

Fig. 3. Ozone profile observed north of 20˚ N during the TRACE-P aircraft mission and model results. Observations are shown in red triangles and the model results as black line.

Title Page

Abstract | Introduction

Conclusions | References

Tables | Figures

◄◄ | ►►

◄ | ►

Back | Close

Full Screen / Esc

Printer-friendly Version

Interactive Discussion
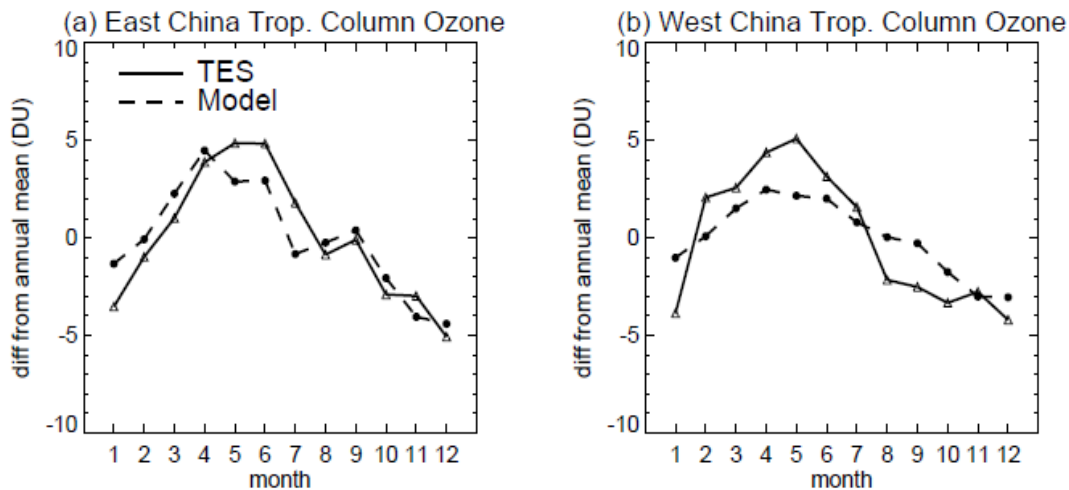
Fig. 4. Month-to-month variations of tropospheric ozone column (TOC) averaged over east **(a)** and west **(b)** China retrieved from TES (solid line) and simulated by the model (dash line). Displayed are TES version 3 level-2 TOC retrievals averaged over three years (2006–2008). Model results are for 2006. The monthly variability is shown by subtracting annual mean TOC from the monthly mean.
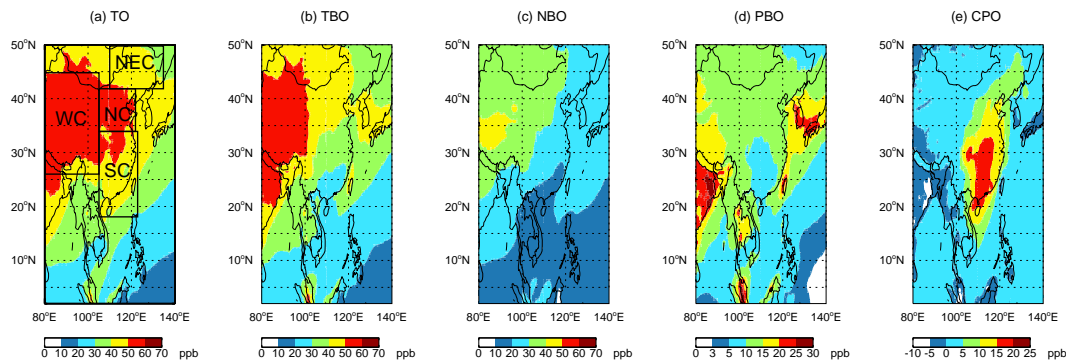
Fig. 5. Annual mean spatial distribution of surface ozone over China. The figure shows the total surface ozone (TO) **(a)**, total background ozone (TBO) **(b)**, natural background ozone (NBO) **(c)**, pollution background ozone (PBO) **(d)**, and China pollution ozone (CPO) **(e)**. Note that the color scales for (d) and (e) are different from those of (a)–(c). The black lines in (a) show the definition of Chinese regions (WC, NEC, NC, and SC).
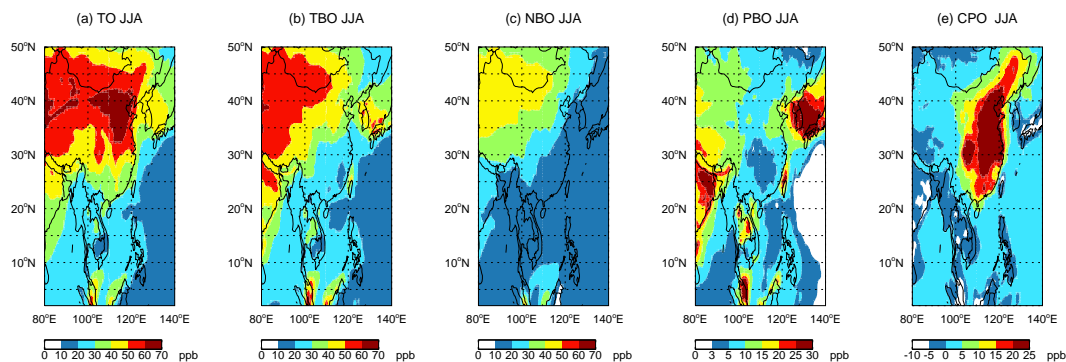
Fig. 6. Same as in Fig. 5, but for summer (June, July and August) mean value.

Fig. 7. Topography (meters) of China.

ACPD

10, 27853–27891, 2010

Seasonal and spatial variability of surface ozone over China

Y. Wang et al.

Title Page

Abstract	Introduction
Conclusions	References
Tables	Figures

| ◄◄ | ►► |
| ◄ | ► |

| Back | Close |

Full Screen / Esc

Printer-friendly Version

Interactive Discussion

Mean lifetime of O$_3$ JJA
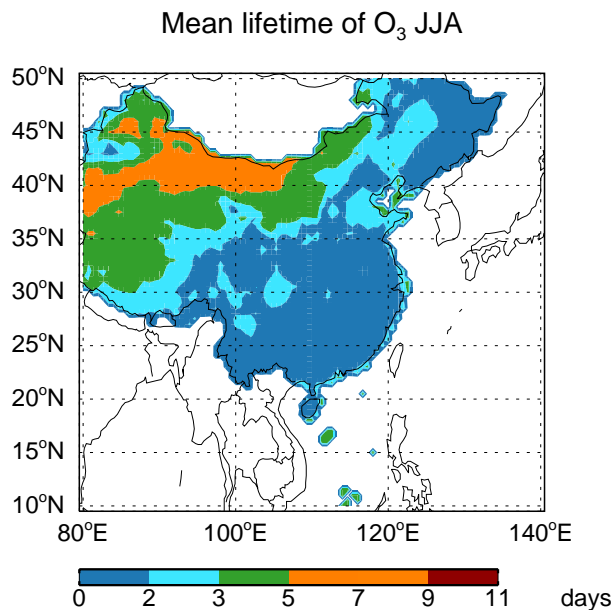
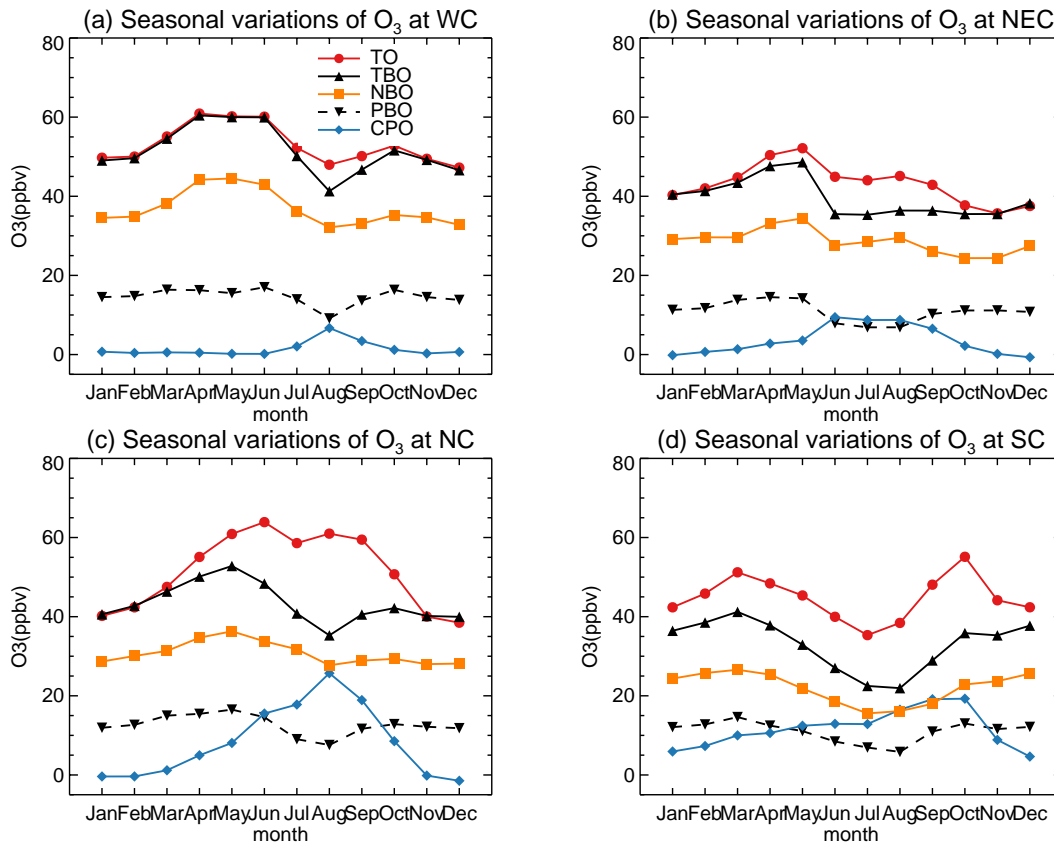**Fig. 8.** Mean lifetime of ozone in the summer (JJA).

Fig. 9. Monthly variations of mean surface ozone (TO, red circles), total background ozone (TBO, solid line with black upward triangles), natural background ozone (NBO, orange squares), pollution background ozone (PBO, dotted line with black downward triangles), and China pollution ozone (CPO, blue diamond) for different Chinese regions. The unit is ppbv. The regions are defined in Fig. 5a.

Title Page

Abstract | Introduction

Conclusions | References

Tables | Figures

|◄ | ►|

◄ | ►

Back | Close

Full Screen / Esc

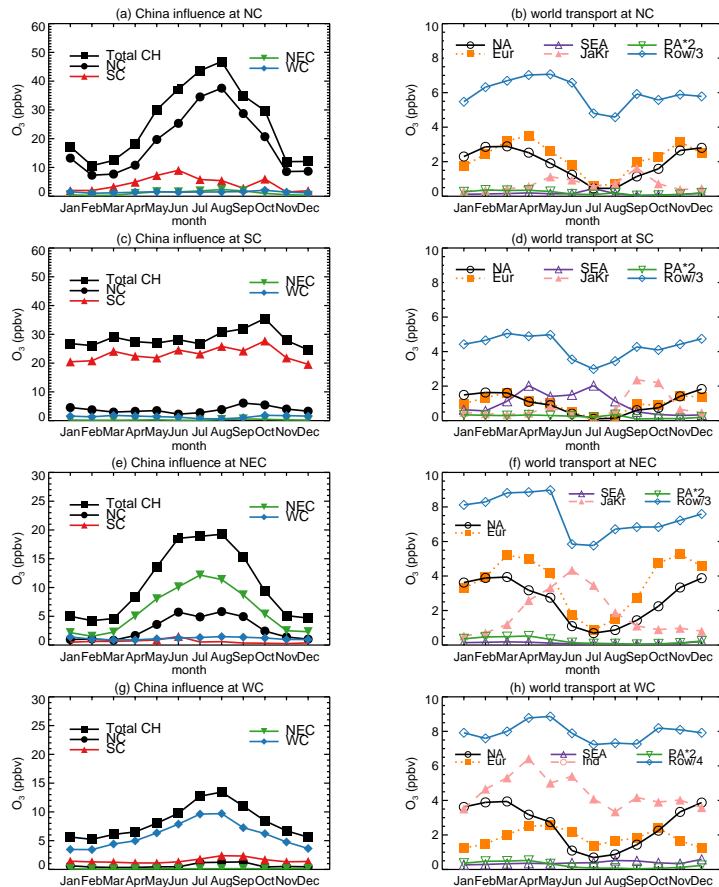Printer-friendly Version

Interactive Discussion

Fig. 10. Monthly mean mixing ratios of tagged ozone tracers over the four Chinese regions. Chinese tracers are shown in the left panel **(a, c, e, g)** and non-Chinese tracers in the right panel **(b, d, f, h)**. For simplicity, tracers with little seasonality or minimal impact on the receptor regions are not displayed in the figure. Note the different scale of the y-axis.

Seasonal and spatial variability of surface ozone over China

Y. Wang et al.

Title Page

Abstract	Introduction
Conclusions	References
Tables	Figures

◄◄ | ►►

◄ | ►

Back | Close

Full Screen / Esc

Printer-friendly Version

Interactive Discussion